J. Astrophys. Astr. (2017) 38: 14
DOI 10.1007/s12036-017-9432-2

Review

Fisher Matrix-based Predictions for Measuring the $z = 3.35$ Binned 21-cm Power Spectrum using the Ooty Wide Field Array (OWFA)

ANJAN KUMAR SARKAR[1,*], SOMNATH BHARADWAJ[1,2] and SK. SAIYAD ALI[3]

[1]Centre for Theoretical Studies, India Institute of Technology Kharagpur, Kharagpur 721 302, India.
[2]Department of Physics, India Institute of Technology Kharagpur, Kharagpur 721 302, India.
[3]Department of Physics, Jadavpur University, Kolkata 700 032, India.
*Corresponding author. E-mail: anjan@cts.iitkgp.ernet.in

MS received 19 July 2016; accepted 20 October 2016; **ePublication**: 17 March 2017

Abstract. We use the Fisher matrix formalism to predict the prospects of measuring the redshifted 21-cm power spectrum in different k-bins using observations with the upcoming Ooty Wide Field Array (OWFA) which will operate at 326.5 MHz. This corresponds to neutral hydrogen (HI) at $z = 3.35$, and a measurement of the 21-cm power spectrum provides a unique method to probe the large-scale structures at this redshift. Our analysis indicates that a 5σ detection of the binned power spectrum is possible in the k range $0.05 \leq k \leq 0.3\,\mathrm{Mpc}^{-1}$ with 1000 hours of observation. We find that the signal-to-noise ratio (SNR) peaks in the k range $0.1-0.2\,\mathrm{Mpc}^{-1}$ where a 10σ detection is possible with 2000 hours of observations. Our analysis also indicates that it is not very advantageous to observe beyond 1000 h in a single field-of-view as the SNR increases rather slowly beyond this in many of the small k-bins. The entire analysis reported here assumes that the foregrounds have been completely removed.

Keywords. Cosmology: large scale structure of the Universe—intergalactic medium—diffuse radiation.

1. Introduction

The redshifted 21-cm emission from the discrete, unresolved neutral hydrogen (HI) sources in the post-reionization era ($z < 6$) appears as a faint diffuse background radiation in low-frequency observations below 1420 MHz. This provides us an useful tool to explore the large scale structure of the Universe in the post-reionization era, using the fluctuations in the diffuse background radiation to trace the HI power spectrum (Bharadwaj *et al.* 2001; Bharadwaj & Sethi 2001). In addition to probing the HI power spectrum (Bharadwaj & Pandey 2003; Bharadwaj & Srikant 2004), fluctuations in the diffuse background radiation also probe the bispectrum (Ali *et al.* 2006; Guha Sarkar & Hazra 2013). In recent years, a considerable amount of work has been done to explore the prospects of detecting the 21-cm HI signal from the post-reionization era (Visbal *et al.* 2009; Bharadwaj *et al.* 2009; Wyithe & Loeb 2009; Seo *et al.* 2010; Mao 2012; Ansari *et al.* 2012; Bull *et al.* 2015).

In the post-reionization era, the bulk of the HI 21-cm emission originates from the dense pockets of self-shielded HI regions, which are identified as damped Lyα (DLA) systems in quasar observations. The fluctuations in the HI 21-cm emission which are in general quantified through HI power spectrum, is expected to trace the matter power spectrum with a possible bias (Bharadwaj *et al.* 2001; Bharadwaj & Sethi 2001). Wyithe & Loeb (2009) have shown that the complications in the HI power spectrum arising due to the modulation of the ionizing field are less than 1%. Bagla *et al.* (2010) have used semi-numerical simulations to predict the HI bias. They have used three different prescriptions to assign HI mass to the dark matter haloes and have found the HI bias to be scale-independent on large scales ($k \leq 1\ \mathrm{Mpc}^{-1}$). Guha Sarkar *et al.* (2012) and Villaescusa-Navarro *et al.* (2015) have used similar simulations and their results are also found to be consistent with a scale-independent HI bias on large scales. Recently, Sarkar *et al.* (2016) have used semi-numerical simulations to model the HI bias and have provided a fitting formula for the HI bias $b_{\mathrm{HI}}(k, z)$ in both k and z across $0.01 \leq k \leq 10\ \mathrm{Mpc}^{-1}$ and $0 \leq z \leq 6$.

The measurement of the HI power spectrum holds the possibility of constraining the background cosmological model through the Baryon Acoustic Oscillations

(BAO) (Wyithe *et al.* 2008; Chang *et al.* 2008). Seo *et al.* (2010) have studied the possibility of measuring BAO using the HI power spectrum with a ground-based radio telescope. The measurement of the HI power spectrum can also be used to constrain cosmological parameters independent of the BAO (Bharadwaj *et al.* 2009; Visbal *et al.* 2009). The measurement of the HI power spectrum can also be used to constrain the neutrino mass (Loeb & Wyithe 2008). Villaescusa-Navarro *et al.* (2015) have used hydrodynamical simulations to study the signatures of massive neutrinos on the HI power spectrum and put constraints on the neutrino mass. In a recent work, Pal & Guha Sarkar (2016) have studied the prospects of measuring the neutrino mass using the HI 21-cm and the Ly-α forest cross-correlation power spectrum.

Measurements of the HI power spectrum are sensitive to both the mean neutral hydrogen fraction $\Omega_{\rm HI}(z)$ and the HI bias $b_{\rm HI}$. Several measurements have been carried out in the past years to measure the value of the $\Omega_{\rm HI}$ both at low and at high redshifts. Measurements of the $\Omega_{\rm HI}$ at low redshifts ($z \leq 1$) come from HI galaxy surveys (Zwaan *et al*. 2005; Martin *et al*. 2010; Delhaize *et al*. 2013), DLAs observations (Rao *et al*. 2006; Meiring *et al*. 2011) and HI stacking (Lah *et al.* 2007; Rhee *et al.* 2013), while measurements of $\Omega_{\rm HI}$ at high redshifts ($1 < z < 6$) are from DLAs studies (Prochaska & Wolfe 2009; Noterdaeme *et al.* 2012; Zafar *et al.* 2013). Measurement of the HI power spectrum can provide astrophysical information about the HI distribution.

Efforts have been made to measure the $\Omega_{\rm HI}$ at redshifts $z < 1$. Chang *et al.* (2010) and Masui *et al.* (2013) have studied the cross-correlation of the HI intensity and the galaxy surveys, while Switzer *et al.* (2013) have studied the autocorrelation of HI intensity to measure the $\Omega_{\rm HI}$. Ghosh *et al.* (2011) have used the GMRT observations to place an upper limit on the value of $\Omega_{\rm HI}$ at $z = 1.33$.

Several low-frequency radio interferometric arrays (CHIME[1], Bandura *et al.* 2014; BAOBAB[2], Pober *et al.* 2013) are planned to measure the BAO using the 21-cm signal from $z \leq 2.55$. Shaw *et al.* (2014) presented theoretical estimates for the sensitivity of CHIME to constrain the line-of-sight and angular scale of the BAO. The Giant Meterwave Radio Telescope (GMRT[3], Swarup *et al.* 1991) operates at frequencies corresponding to HI in the redshift range $0 \leq z \leq 8.5$. The GMRT is currently being upgraded. The prospects of detecting the HI power spectrum from the post reionization era for the upgraded GMRT (uGMRT) has been studied in Chatterjee *et al.* (2017). The proposed future telescopes SKA1-mid and SKA1-low[4], both hold the prospect of measuring the post-reionization HI power spectrum at a high level of precision (Guha Sarkar & Datta 2015; Bull *et al.* 2015; Santos *et al.* 2014).

There is a rich literature on the sensistivity estimates for various low frequency radio telescopes. Morales (2005) presented a general method to calculate the Epoch of Reionization (EoR) power spectrum sensitivity for any radio-interferometric array. Harker *et al.* (2010) have made sensitivity estimates for the Low Frequency Array (LOFAR[5], van Haarlem *et al.* 2013). Similar estimates have been made in the context of the Murchison Wide-field Array (MWA[6], Bowman *et al.* 2013; Tingay *et al.* 2013). Beardsley *et al.* (2013) have estimated the sensitivity of the MWA to the EoR 21-cm power spectrum and McQuinn *et al.* (2006) presented estimates for cosmological parameter estimation using MWA5000, a hypothetical extended version of MWA. Parsons *et al*. (2012) have explored redundancy calibration in the context of the Donald C. Backer Precision Array to Probe the Epoch of Reionization (PAPER[7], Parsons *et al.* 2010). Pober *et al.* (2014) have studied the constraints achievable with the Hydrogen Epoch of Reionization Array (HERA[8], DeBoer *et al.* 2016; Neben *et al.* 2016) and have found that very high significance ($\gtrsim\sim 30\sigma$) detection of the reionization power spectrum is possible in even the most pessimistic scenarios. Ewall-Wice *et al.* (2016) have used the Fisher matrix formalism to predict the sensitivity with which it will be possible to constrain reionization and X-ray heating models with the future HERA and SKA phase I.

Here, we discuss the prospects of measuring the HI power spectrum at $z \sim 3$, using the upgraded Ooty radio Telescope (ORT). The ORT consists of a 530-m long and 30-m wide parabolic cylindrical reflector, which is placed in the North–South direction on a hill having the same slope as the latitude (11°) of the station (Swarup *et al.* 1971; Sarma *et al.* 1975). It is possible to observe the same part of the sky through a single rotation of the long axis, which is aligned with the Earth's

[1] http://chime.phas.ubc.ca/
[2] http://bao.berkeley.edu/
[3] http://gmrt.ncra.tifr.res.in/
[4] https://www.skatelescope.org/home/technicaldatainfo/key-documents/
[5] http://www.lofar.org/
[6] http://www.mwatelescope.org
[7] http://astro.berkeley.edu/dbacker/eor
[8] http://reionization.org/

rotation axis. The entire feed system of the ORT has 1056 dipoles, spaced 0.47 m apart from each other, which are placed along the focal line of the telescope. The cylindrical Ooty Radio Telescope (ORT) is currently being upgraded (Prasad & Subrahmanya 2011a, b, 2014; Subrahmanya *et al*. 2017a, b) to function as a linear radio interferometric array, the Ooty Wide Field Array (OWFA). The OWFA works at a nominal frequency of $\nu_0 = 326.5$ MHz, which corresponds to HI radiation from the redshift $z = 3.35$. The OWFA can operate in two independenet interferometric modes – Phase I and Phase II. In this work, we have considered Phase II only. The Phase II has 264 antenna elements, where each antenna element consists of four dipoles. Each antenna has a rectangular aperture of dimension 1.92 m $\times$ 30 m. The field-of-view of OWFA Phase II is highly assymetric in dimension, $27.4^\circ \times 1.75^\circ$. The operating bandwidth for the Phase II is 40 MHz. The field-of-view and the observing bandwidth of the OWFA Phase II allow to observe the Universe over a real space volume $\sim 0.3\,\mathrm{Gpc}^3$.

We now report some recent works related to OWFA. Calibration is an important issue for OWFA and it has been addressed in Marthi & Chengalur (2014). Ghelot & Bagla (2017) have followed the approach of Ali & Bharadwaj (2014) to predict the HI signal expected at OWFA. Marthi (2017) presented a programmable emulator for simulating OWFA observations for which foreground modelling and predictions are presented in Marthi *et al.* (2017). Chatterjee *et al.* (2017) presented simulations of the HI signal expected at OWFA.

Ali & Bharadwaj (2014) (hereafter, Paper I) have studied the prospects of detecting the 21-cm signal using OWFA. In this paper, we have also made detailed foreground predictions for OWFA. In a recent study, Bharadwaj *et al.* (2015) (hereafter, Paper II) have used the Fisher matrix analysis to make predictions for hours of observations to measure the HI power spectrum. We showed that the dominant contribution to the OWFA HI signal is from the k-range $0.02 \le k \le 0.2$ Mpc^{-1}. It was found that a 5σ detection of the HI power spectrum is possible with ~ 150 h of observations using Phase II. In this study, we have also explored the possibility of measuring the redshift space distortion parameter β. We found that the non-uniform sampling of the **k**-modes does not make OWFA suitable for measuring β.

The predictions for OWFA, mentioned earlier, have all assumed that the HI power spectrum is related to the ΛCDM power spectrum with a scale-independent linear HI bias. All of these studies have focussed on measuring the amplitude of the HI power spectrum assuming that the shape of the matter power spectrum (Eisenstein & Hu 1998) is precisely known. It is interesting and worthwhile to consider a situation where both amplitude and the shape of the HI power spectrum is unknown. There are several astrophysical processes which could, in principle, change the shape of the HI power spectrum without affecting the matter power spectrum. Further, uncertainties in the background cosmological model would also be reflected as changes in the observed HI power spectrum through various effects like redshift space distortion and Alcock–Paczynski (AP) effect. In this paper, we have considered the possibility of measuring the HI power spectrum using OWFA. For this purpose, we have divided the k-range into several bins and employed the Fisher matrix analysis to make predictions for measuring the HI power spectrum in each of these k-bins. Throughout our analysis, we have used the ΛCDM cosmology with PLANCK+WMAP9 best-fit cosmological parameters (Ade *et al.* 2014).

The paper is structured as follows. In section 2, we present the theoretical HI model which was used for calculating the signal and noise covariance. Here we also show the Fisher matrix technique which was employed for estimating the binned HI power spectrum. In section 3, we use the results from the Fisher matrix analysis to make predictions for measuring the binned 21-cm power spectrum. In Section 4, the summary and conclusions are given.

2. Visibility covariance and Fisher matrix

OWFA measures visibilities $\mathcal{V}(\mathbf{U}_a, \nu_n)$ at given baselines $\mathbf{U}_a$ and frequency channel ν_n. The baseline configuration of the OWFA is one-dimensional. It consists of 264 antennas, arranged in a linear array along the length of the cylinder. Assuming the x-axis to be along the length of the cylinder, the baselines of the OWFA can be written as

$$\mathbf{U}_a = a\left(\frac{d}{\lambda}\right)\hat{i} \quad (1 \le a \le 263), \tag{1}$$

where a denotes the baseline number, $d = 1.92$ m, is the distance between two consecutive antennas and λ is the wavelength corresponding to the central observing frequency ν_0. OWFA has a high degree of redundancy in baselines. For OWFA, any given baseline $\mathbf{U}_a$ occurs $(264 - a)$ times in the array. This can be used to both calibrate the antenna gains (independent of the

sky model) as well as to estimate the true visibilities (Marthi & Chengalur 2014).

In reality baselines $\mathbf{U}_a$ change as frequency varies across the observing bandwidth (B). This is an extremely important factor that needs to be taken into account in the actual data analysis. The expected fractional variation in the baseline $\Delta U/U$, about the central frequency ν_0 over the bandwidth of observation is $\Delta U/U = B/2\nu_0 \sim 4.5\%$ for $B = 30$ MHz. This is not significant enough to consider in our analysis and we have kept the baselines fixed at the value, corresponding to the central frequency ν_0. The actual bandwidth may be somewhat larger than $B = 30$ MHz.

We express the telescope's observing frequency bandwidth as $B = N_c \Delta\nu_c$ where N_c is the number of the frequency channels and $\Delta\nu_c$ is the channel-width. For our analysis, we have used $N_c = 300$ with $\Delta\nu_c = 0.1$ MHz.

The measured visibilities $\mathcal{V}(\mathbf{U}_a, \nu_n)$ can be expressed as of sum of the HI signal $\mathcal{S}(\mathbf{U}_a, \nu_n)$ and the noise $\mathcal{N}(\mathbf{U}_a, \nu_n)$, i.e.,

$$\mathcal{V}(\mathbf{U}_a, \nu_n) = \mathcal{S}(\mathbf{U}_a, \nu_n) + \mathcal{N}(\mathbf{U}_a, \nu_n) \tag{2}$$

assuming that foregrounds have been completely removed from the data.

For the Fisher matrix analysis, it is of convenience to decompose the visibilities $\mathcal{V}(\mathbf{U}_a, \nu_n)$ into delay channels τ_m (Morales 2005) rather than frequency channels ν_n, i.e.,

$$v(\mathbf{U}_a, \tau_m) = \Delta\nu_c \sum_{n=1}^{N_c} \mathrm{e}^{2\pi i \tau_m \nu_n}\, \mathcal{V}(\mathbf{U}_a, \nu_n), \tag{3}$$

where τ_m is the delay channel which is defined as

$$\tau_m = \frac{m}{B} \quad \text{with} \quad \frac{N_c}{2} < m \leq \frac{N_c}{2}. \tag{4}$$

The visibilities $v(\mathbf{U}_a, \tau_m)$ and $v(\mathbf{U}_b, \tau_n)$ are uncorrelated for $m \neq n$ (Paper II). It is therefore necessary to only consider the visibility correlations with $m = n$ for which we define the visibility covariance matrix

$$C_{ab}(m) = \langle v(\mathbf{U}_a, \tau_m) v^*(\mathbf{U}_b, \tau_m) \rangle\,. \tag{5}$$

The visibility covariance matrix $C_{ab}(m)$ can be expressed in terms of the redshifted HI 21-cm brightness temperature power spectrum $P_{\mathrm{T}}(\mathbf{k}_\perp, k_\parallel)$ as (eq. (5) of Paper II)

$$C_{ab}(m) = \frac{B}{r_\nu^2 r'_\nu} \left(\frac{2k_{\mathrm{B}}}{\lambda^2}\right)^2 \int d^2U'\, \tilde{A}(\vec{U}_a - \vec{U}')\, \tilde{A}^*(\vec{U}_b - \vec{U}') \times P_{\mathrm{T}}(\mathbf{k}_\perp, k_\parallel) + \frac{2\Delta\nu_c B \sigma_N^2}{(264 - a)} \delta_{a,b}, \tag{6}$$

where the first and the second terms refer to the signal and noise covariance respectively. Here r_ν is the comoving distance between the observer and the region of space from where the HI radiation originated, $r'_\nu = \frac{dr_\nu}{d\nu}$ gives the conversion factor from frequency to comoving distance ($r_\nu = 6.85$ Gpc and $r'_\nu = 11.5$ Mpc MHz^{-1} for OWFA) and $\tilde{A}(\mathbf{U})$ is the Fourier transform of the OWFA primary beam pattern (equation (6) of Paper I)). The factor $\frac{2k_{\mathrm{B}}}{\lambda^2}$ gives the conversion from brightness temperature to specific intensity (where k_{B} is the Boltzmann constant), $P_{\mathrm{T}}(\mathbf{k}_\perp, k_\parallel)$ is the redshifted HI 21-cm brightness temperature power spectrum, $\mathbf{k}_\perp = \pi(\mathbf{U}_a + \mathbf{U}_b)/r_\nu$ and $k_\parallel = 2\pi\tau_m/r'_\nu$ respectively refer to the perpendicular and parallel components of the wave vector $\mathbf{k}$ with $k = \sqrt{k_\perp^2 + k_\parallel^2}$ (Bharadwaj *et al.* 2015). The rms noise of the measured visibilities has contribution from the system noise and has a value $\sigma_N = 6.69$ Jy for 16 s integration time (Table 1 of Paper I) and the factor $(264 - a)^{-1}$ in the noise contribution accounts for the redundancy in the baseline distribution for OWFA.

For OWFA, the visibilities at any two baselines $\mathbf{U}_a$ and $\mathbf{U}_b$ are uncorrelated ($C_{ab}(m) = 0$) if $|a - b| > 1$ ie. the visibility at a particular baseline $\mathbf{U}_a$ is only correlated with the visibilities at the same baselines or the adjacent baselines $\mathbf{U}_{a\pm1}$. Thus, for a fixed m, $C_{ab}(m)$ is a symmetric, tridiagonal matrix where the diagonal represents the visibility correlation at the same baseline whereas the upper and lower diagonals represent the visibility correlation between the adjacent baselines. Figure 1 of Paper II shows the signal contribution for the diagonal and off-diagonal terms of $C_{ab}(m)$. The covariance at adjacent baselines is approximately one fourth of the covariance at the same baselines. Further, the noise contributes only to the diagonal terms and it does not figure in the off-diagonal terms.

We have used the Fisher matrix (equation (8) of Paper II)

$$F_{\alpha\gamma} = \frac{1}{2} \sum_m C_{ab}^{-1}(m) [C_{bc}(m)]_{,\alpha} C_{cd}^{-1}(m) [C_{da}(m)]_{,\gamma} \tag{7}$$

to predict the accuracy with which it will be possible to constrain the value of various parameters using observations with OWFA. The indices α, γ here refer to the different parameters whose values we wish to constrain. The inverse of the Fisher matrix $F_{\alpha\gamma}$ provides an estimate of the error-covariance (Dodelson 2003) for these parameters. In equation (7), the indices a, b, c, d are to be summed over all baselines. We have used equation (6) to calculate the data covariance matrix $C_{ab}(m)$ and also its derivatives $[C_{ab}(m)]_{,\alpha}$ with respect

to the parameters whose values we wish to constrain. A discussion of the parameters considered for the present analysis follows in the next section.

3. Modelling and binning the HI power spectrum

The redshifted HI 21-cm brightness temperature power spectrum $P_{\rm T}(\mathbf{k})$ is the quantity that will be directly measured by any cosmological 21-cm experiment. This quantifies the fluctuations in the brightness temperature originating from two different sources: (1) the intrinsic fluctuations of the HI density in real co-moving space and (2) the peculiar velocities which introduce brightness temperature fluctuations through redshift space distortion. For the purpose of this work, we have modelled $P_{\rm T}(\mathbf{k})$ as

$$P_{\rm T}(\mathbf{k}) = (1+\beta\mu^2)^2 P_{\rm T}^r(k), \tag{8}$$

where $P_{\rm T}^r(k)$ is the power spectrum of the HI 21-cm brightness temperature fluctuations in real space and the factor $(1+\beta\mu^2)^2$ quantifies the effect of linear redshift space distortion due to peculiar velocities (Kaiser 1987; Bharadwaj *et al.* 2001; Ali & Bharadwaj 2014). Here β is the redshift space distortion parameter and $\mu = k_\parallel/k$.

OWFA will probe the $k_\perp$ and $k_\parallel$ range $1.9\times10^{-3} \le k_\perp \le 5\times10^{-1}$ Mpc^{-1} and $1.8\times10^{-2} \le k_\parallel \le 2.73$ Mpc^{-1} respectively, thereby covering the k-range $1.82\times10^{-2} \le k \le 2.73$ Mpc^{-1}. The present work focusses on making predictions for the accuracy with which it will be possible to measure $P_{\rm T}^r(k)$ using OWFA. For this purpose, we have divided the entire k-range probed by OWFA into 20 equally spaced logarithmic k-bins, and we use k^i and $[P_{\rm T}^r]^i$ (with $1 \le i \le 20$) to refer respectively to the average k and $P_{\rm T}^r(k)$ value for each bin. We have used $\ln([P_{\rm T}^r]^i)$ and $\ln(\beta)$ as the parameters for the Fisher matrix analysis (equation (7)) which gives an estimate of the precision with which it will be possible to measure these parameters.

4. Results and discussion

We need a fiducial model for the $P_{\rm T}^r(k)$ and β to carry out the Fisher matrix analysis. We model the $P_{\rm T}^r(k)$ assuming that it traces the underlying matter power spectrum $P(k)$ with a linear bias $b_{\rm HI}$ as also assumed by Bharadwaj *et al.* (2001), Bharadwaj & Sethi (2001), Wyithe & Loeb (2009),

$$P_{\rm T}^r(k) = (\bar{x}_{\rm HI}\, b_{\rm HI}\, \bar{T})^2\, P(k), \tag{9}$$

where $\bar{x}_{\rm HI}$ is the mean neutral hydrogen fraction. The characteristic HI brightness temperature $\bar{\rm T}$ is defined as (Bharadwaj & Ali 2004)

$$\bar{T}(z) = 4.0\,{\rm mK}\,(1+z)^2 \times \left(\frac{1-Y_P}{0.75}\right)\left(\frac{\Omega_b h^2}{0.020}\right)\left(\frac{0.7}{h}\right)\left(\frac{H_0}{H(z)}\right), \tag{10}$$

where Y_P is the helium mass fraction and the other symbols in the above equation have their usual meanings.

The parameter β in the observed $P_{\rm T}(k)$ (equation (9)) is defined as $\beta = f(\Omega)/b_{\rm HI}$ where $f(\Omega)$ quantifies the growth rate of the matter density perturbations, whose value is specified by the background ΛCDM cosmological model. Note that the various terms used in equation (9) correspond to the redshift, $z = 3.35$ where HI radiation originated.

We have used $\bar{x}_{\rm HI} = 0.02$ for our analysis which corresponds to the neutral gas mass density parameter $\Omega_{\rm gas} = 10^{-3}$. This value of $\Omega_{\rm gas}$ comes from DLA observations in the redshift range of our interest (Prochaska & Wolfe 2009; Noterdaeme *et al.* 2012; Zafar *et al.* 2013). Simulations (Bagla *et al.* 2010; Guha Sarkar *et al.* 2012; Sarkar *et al.* 2016) and analytical modelling (Martin *et al.* 2010) suggest the use of a constant, scale-independent bias at wave numbers $k \le 1$ Mpc^{-1}, and we use the value $b_{\rm HI} = 2.0$ for our entire analysis. We use these values and the cosmological parameters to calculate the fiducial values of $[P_{\rm T}^r]^i$ (points in Fig. 2) and $\beta = 4.93\times10^{-1}$.

The value of β can be estimated by sampling the Fourier modes $\mathbf{k}$ with a fixed magnitude k which are, however, oriented at different directions to the line-of-sight. In other words, $\mu = k_\parallel/k$ should uniformly span over the entire range $-1 \le \mu \le 1$. The minimum value of $k_\parallel$ probed by OWFA is approximately 10 times larger than the minimum value of $k_\perp$. The maximum value of $k_\parallel$ is also ∼4 times larger than the maximum value of $k_\perp$ (Table II of Paper II). In addition to this, the sampling width for $k_\parallel$ is roughly ∼20 times larger than that of $k_\perp$. These disparities lead to a non-uniform distribution where the $\mathbf{k}$ modes are largely concentrated around $\mu = 1$ (see Fig. 3 of Paper II). This anisotropic distribution of the $\mathbf{k}$ modes does not make OWFA very suitable for measuring β, and we do not consider this in our analysis.

We have considered two different cases for error predictions. In the first situation, we consider the conditional errors σ_{ic} for the measurement of the binned HI power spectrum $[P_{\rm T}^r]^i$. The conditional error σ_{ic} represents the error on the measurement of $[P_{\rm T}^r]^i$ in a situation where the values of all the other parameters

are precisely known. Here, we calculate σ_{ic} for the i-th bin by assuming that the values of β and $[P_{\rm T}^r]^j$ are precisely known for all the other bins. We use $\sigma_{ic} = 1/\sqrt{F_{ii}}$ to compute the conditional error for the i-th bin.

In the second situation, we have considered the marginalized errors σ_{im} for the measurement of $[P_{\rm T}^r]^i$. The marginalized error σ_{im} gives the error on the measurement of $[P_{\rm T}^r]^i$ without assuming any prior information about the other parameters. While estimating the error for the i-th bin, we have marginalized over the values of β and $[P_{\rm T}^r]^j$ in the other bins. In our previous work (Paper II), we have calculated the marginalized error on the measurement of the amplitude of the HI power spectrum with a prior on β in the range $0.329 \leq \beta \leq 0.986$. In the present work, we have not imposed any prior on β and we have marginalized $\ln([P_{\rm T}^r]^i)$ and $\ln(\beta)$ over the entire range $-\infty$ to $+\infty$. We use $\sigma_{im} = \sqrt{[F^{-1}]_{ii}}$ to calculate the marginalized error for the i-th bin. The conditional and the marginalized errors here represent the two limiting cases, and the error estimates would lie somewhere in between σ_{ic} and σ_{im} if we impose priors on the value of β or any of the other parameters.

In Paper II, we have shown that a 5σ detection of the amplitude of the $P_{\rm T}^r$ is possible with ∼150 hours of observations. We therefore need to consider an observing time $t > 150$ h for measuring the $[P_{\rm T}^r]^i$ in different k-bins. Figure 1 shows both the conditional (σ_{ic}) and marginalized (σ_{im}) errors for 1000 hours of observation. Here σ_{ic} and σ_{im} are respectively the conditional and marginalized errors for different $\ln([P_{\rm T}^r]^i)$ which are the parameters for the Fisher matrix analysis. Here σ_{ic} and σ_{im} represent the two limiting cases for the error estimates. We expect the error estimates to lie between these two limiting values in case we impose a prior on the value of β (Paper II).

We find that the values of σ_{ic} and σ_{im} agree within 15%, except at the k-bins lying in the range $0.06 \leq k \leq 0.3$ Mpc^{-1} where the difference is ∼20−35%. This suggests that $\sigma_{ic} = 1/\sqrt{F_{ii}}$ and $\sigma_{im} = \sqrt{[F^{-1}]_{ii}}$ are not significantly different, indicating that the contribution from the off-diagonal terms of F_{ij} are small. We therefore conclude that the measurements of $P_{\rm T}^r$ in different k-bins are by and large uncorrelated. In subsequent analysis, we have used σ_{ic} for predicting errors on the measurements of $[P_{\rm T}^r]^i$ in different k-bins.

Figure 2 shows the binned HI power spectrum $[P_{\rm T}^r]^i$ with the 1σ errors $\Delta[P_{\rm T}^r]^i = \sigma_{ic} \times [P_{\rm T}^r]^i$ for 1000 hours of observation. The error $\Delta[P_{\rm T}^r]^i$ on the measurement of the $P_{\rm T}^r$ in a given k-bin is the combination of contributions from the system noise and the cosmic variance. The noise term in equation (6) is suppressed by the factor $(264 - a)^{-1}$ due to the redundancy of the OWFA baselines. We see that the noise contribution goes up as the baseline number a is increased. The small k-bins which correspond to small baselines, have smaller noise contribution than the larger k-bins which correspond to large baselines. Here we have used logarithmic binning where the bin width and the number of k-modes in a bin increase with k. The cosmic variance in a given k-bin goes down with number of k-modes in that bin. We therefore expect the cosmic variance to be maximum at the smallest k-bin and decrease with increasing k. As a whole the errors at smaller k-bins are dominated by the cosmic variance whereas at larger k-bins, the errors are dominated by the system noise.

We can see from Fig. 1 that $\sigma_{ic} = \Delta[P_{\rm T}^r]^i/[P_{\rm T}^r]^i$, which is the relative error on the binned power spectrum, is minimum in the range $k \sim 0.1-0.2\,{\rm Mpc}^{-1}$. The cosmic variance dominates the relative error at smaller values of k ($<0.1\,{\rm Mpc}^{-1}$) whereas the system

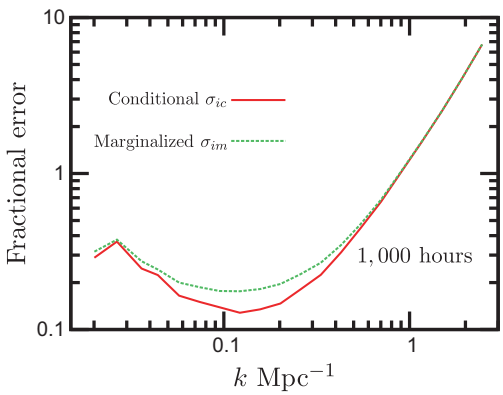

Figure 1. The figure shows the fractional errors for the measurement of $\ln([P_{\rm T}^r]^i)$ in different k-bins with 1000 hours of observation for two situations, conditional σ_{ic} (red solid line) and marginalized σ_{im} (green dashed line) errors.

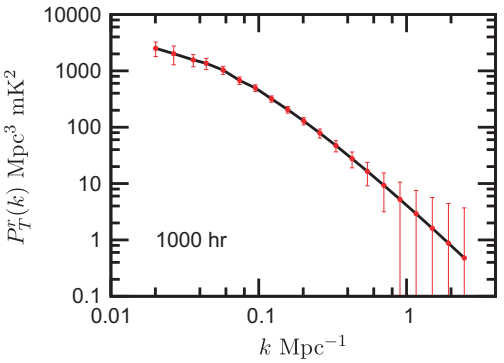

Figure 2. The binned HI power spectrum $[P_{\rm T}^r]^i$ (points) with 1σ errors (vertical bars) for 1000 hours of observation.

noise dominates at larger k values ($>0.2\,\mathrm{Mpc}^{-1}$). We also see that the relative error is lower than 0.2 in the range $0.05 \leq k \leq 0.3\,\mathrm{Mpc}^{-1}$ where our results predict a 5σ detection of the binned power spectrum (Fig. 2).

We have so far considered the errors on the measurement of $[P_{\mathrm{T}}^r]^i$ with given hours of observing time (1000 h). We shall now try to understand how the errors σ_{ic} vary with observation time t. The time dependence of the visibility covariance $C_{ab}(m)$ (equation (6)) comes in through the rms noise of the measured visibilities σ_N which scales inversely with $\sqrt{t}$, i.e. $\sigma_N \sim 1/\sqrt{t}$. We expect the visibility covariance $C_{ab}(m)$ to vary inversely with t, i.e. $C_{ab}(m) \sim 1/t$ for small observing times where the noise contribution is considerably larger than the signal, and we expect $C_{ab}(m)$ to have a constant value, independent of the observing time, for large values of t. The derivatives of the $C_{ab}(m)$ which appear in the Fisher matrix (equation (7)) are independent of t. It then follows that the Fisher matrix $F_{\alpha\gamma}$ scales as $F_{\alpha\gamma} \sim t^2$ for small observation times and $F_{\alpha\gamma}$ has a constant value for large t. We therefore expect the relative errors σ_{ic} to vary as $\sigma_{ic} \sim 1/t$ for small observing times, and become independent of t for large observation times where the error is dominated by the cosmic variance.

Figure 3 shows a contour plot of the signal-to-noise ratio (SNR)

$$\mathrm{SNR} = \frac{1}{\sigma_{ic}} = \frac{[P_{\mathrm{T}}^r]^i}{\Delta[P_{\mathrm{T}}^r]^i}, \tag{11}$$

as functions of the Fourier mode k and observation time t. We see that a statistically significant measurement (3σ) of the binned power spectrum is only possible for observation times greater than 200 h. A 3σ detection of $[P_{\mathrm{T}}^r]^i$ is possible in the k-range $0.04 \leq k \leq 0.2\ \mathrm{Mpc}^{-1}$ with 200–300 hours of observation. Detection at a significance of 5σ is not possible with $t \leq 500$ hours of observation. We find that a 5σ detection of $[P_{\mathrm{T}}^r]^i$ is possible for $0.05 \leq k \leq 0.3\ \mathrm{Mpc}^{-1}$ with 1000 hours of observing time. Note that the SNR peaks in the range $k \sim 0.1$–$0.2\ \mathrm{Mpc}^{-1}$. In this k range the SNR continues to increase with t for the entire t range shown here and a 10σ detection is possible with 2000 hours of observation. At $k < 0.1\,\mathrm{Mpc}^{-1}$, the SNR stops increasing with t beyond a certain point. The SNR here becomes dominated by the cosmic variance as t is increased, and the SNR contour becomes parallel to the t axis. We see that irrespective of the observing time, a 5σ detection is not possible for $k < 0.036\,\mathrm{Mpc}^{-1}$, if only one pointing is considered. For $k > 0.2\,\mathrm{Mpc}^{-1}$, the error is system noise dominated, and the SNR continues to increase with increasing t. However, we see that a 5σ detection is not possible for $k > 0.5\,\mathrm{Mpc}^{-1}$ within 2000 hours of observation.

As mentioned earlier, we expect SNR $\propto t$ for small observing times when the error is system noise dominated, and we expect the SNR to saturate at a fixed value for large observing times where the cosmic variance dominates. Figure 4 shows how the SNR changes with observing time t for a few representative k-bins. The small k bins have a relatively large cosmic variance. We see that the SNR at the smallest k bin ($0.036\,\mathrm{Mpc}^{-1}$) shown in this figure is nearly saturated at a very small observing time ($t \sim 300$ h), and increases very slowly for larger observing times. A 5σ detection in this bin requires $\sim$10000 hours of observation. The k-bin at $0.33\,\mathrm{Mpc}^{-1}$ shows the SNR $\propto t$ scaling for $t \leq 700$ h, beyond which the increase in SNR is slower. The two larger k-bins show the SNR $\propto t$ behaviour over the entire t range considered here. However, note that the largest k-bin with $k^i = 1.16\,\mathrm{Mpc}^{-1}$ shown in the figure has a rather low SNR,

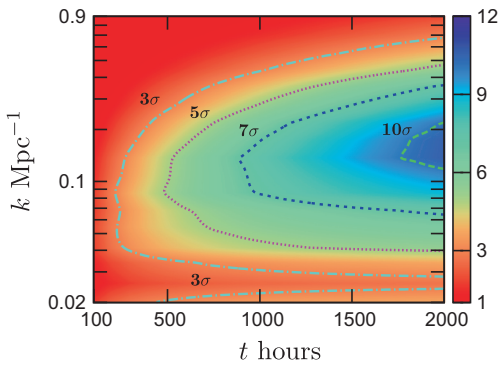

Figure 3. The SNR contours as a function of k-bin and observation time t.

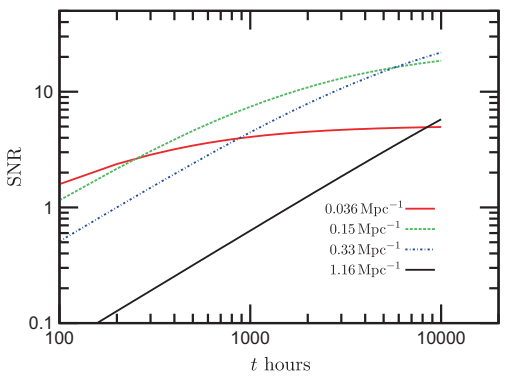

Figure 4. The signal-to-noise ratio (SNR) with observation time t for different k^i values (mentioned in the figure).

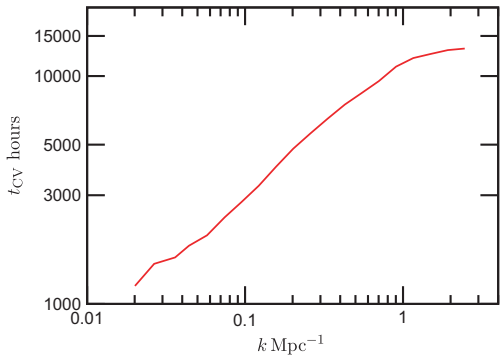

Figure 5. The observation time (t_{CV}) at which the cosmic variance starts to dominate the error on the measurement of the HI power spectrum for different k-bins.

and a 5σ detection is only possible with 10000 hours of observation.

As mentioned earlier, we expect the SNR to increase with time t, i.e. SNR $\propto t$ for small observing times. The increase in the SNR slows down for larger observing times, and for even larger observing times ($t \geq t_{CV}$) the SNR saturates at a fixed value which is determined by the cosmic variance in the particular k-bin. Here t_{CV} refers to the observing time beyond which the SNR is determined by the cosmic variance, and we have estimated this for the different k bins such that the SNR increases slower than $t^{0.002}$ for ($t \geq t_{CV}$). Figure 5 shows t_{CV} for the different k-bins. For any particular bin, it is not possible to increase the SNR any further by increasing the observing time beyond t_{CV}. We find that t_{CV} increases approximately as $t_{CV} \propto k^{0.63}$ for $k \leq 1.0\,\mathrm{Mpc}^{-1}$. The increase in the t_{CV} is rather slow for $k \geq 1\,\mathrm{Mpc}^{-1}$ and saturates at $t_{CV} \sim 15000\,\mathrm{h}$ beyond $k = 2.0\,\mathrm{Mpc}^{-1}$. This behaviour is decided by a combination of several factors including the OWFA baseline redundancy, the sampling of the 3D Fourier modes and the logarithmic binning.

The discussion till now has entirely focused on observations in a single field-of-view. As already mentioned, the SNR ceases to increase with observing time once $t \sim t_{CV}$. We see that $t_{CV} \sim 1000\,\mathrm{h}$ at the smallest k bin. The SNR in this bin will saturate for $t > 1000\,\mathrm{h}$ and it is necessary to observe multiple fields-of-view to increase the SNR any further. The SNR scales as SNR $\propto \sqrt{N}$, where N is the number of fields-of-view. A possible observational strategy for OWFA would be to observe multiple fields-of-view, with each field being observed for a duration of 1000−2000 h. The 3σ contour in Fig. 3 would correspond to 5.2σ for observations in $N = 3$ fields-of-view. We see that a 5σ detection is possible in nearly all the k bins if three fields-of-view are observed for 1500 h each.

5. Summary and conclusions

We have considered Phase II of OWFA to study the prospects of measuring the redshifted 21-cm power spectrum in different k-bins. The entire analysis is restricted to observations in a single field-of-view. We find that a 5σ detection of the binned power spectrum is possible in the k range $0.05 \leq k \leq 0.3\,\mathrm{Mpc}^{-1}$ with 1000 hours of observation. The SNR peaks in the k range 0.1–0.2 Mpc^{-1} where a 10σ detection is possible in 2000 hours of observation. Our study reveals that it is not very advantageous to observe much beyond 1000 h as the error in measuring the power spectrum become cosmic variance dominated in several of the small k-bins, and the SNR in these bins increase rather slowly with increasing t.

As discussed earlier, the variation of the baseline over the observing bandwidth is ∼5%. This makes both the diagonal and off-diagonal components of the Fisher matrix to change, which is expected to be not more than 5−10%.

The redshifted 21-cm signal provides an unique way to measure the BAO in the post-reioinization era ($z \leq 6$). This is perceived to be a sensitive probe of the dark energy. The BAO is a relatively small feature (∼10−15%) that sits on the HI power spectrum. The five successive peaks of the BAO span the k range $0.045 \leq k \leq 0.3$ Mpc^{-1}, which is well within the k-range probed by OWFA. The detection of the BAO requires measuring the HI power spectrum at a significance of 50σ or more. From Fig. 3, we find that such a sensitivity cannot be achieved in the relevant k range within $t \sim 2000$ hours of observation. It is also clear that the required sensitivity cannot be achieved by considering observations in a few fields-of-view. For detecting the BAO, it is necessary to consider a different observational strategy covering the entire sky (e.g. Shaw *et al.* 2015). We plan to address this in future work.

Acknowledgements

The authors acknowledge Jayaram N. Chengalur, Jasjeet S. Bagla, Tirthankar Roy Choudhury, C. R. Subrahmanya, P. K. Manoharan and Visweshwar Ram Marthi for helpful discussions. AKS would like to acknowledge Rajesh Mondal and Suman Chatterjee for their help. AKS would like to specially mention Debanjan Sarkar for a detailed reading of the manuscript and providing important suggestions. AKS would also like to thank the anonymous referees whose critical suggestions helped in the improvement of the language and presentation of the manuscript. SSA would

like to acknowledge CTS, IIT Kharagpur for the use of its facilities and thank the authorities of IUCAA, Pune, India for providing the Visiting Associateship programme.

References

Ade, P. A. R., Aghanim, N. *et al.* 2014, *A&A*, **571**, A16.

Ali, S. S., Bharadwaj, S., Pandey, S. K. 2006, *MNRAS*, **366**, 213.

Ali, S. S., Bharadwaj, S. 2014, *J. Astrophys. Astr.*, **35**, 157.

Ansari, R., Campagne, J. E., Colom, P. *et al.* 2012, *A&A*, **540**, A129.

Bagla, J. S., Khandai, N., Datta, K. K. 2010, *MNRAS*, **407**, 567.

Bandura, K., Addison, G. E., Amiri, M. *et al.* 2014, *Proc. SPIE 9145 Ground-based and Airborne Telescopes V,* 914522.

Beardsley, A. P., Hazelton, B. J., Morales, M. F. *et al.* 2013, *MNRASL*, **429**, L5.

Bharadwaj, S., Sethi, S., Saini, T. D. 2009, *Phys. Rev. D*, **79**, 083538.

Bharadwaj, S., Ali, S. S. 2004, *MNRAS*, **352**, 142.

Bharadwaj, S., Nath, B. N., Sethi, S. K. 2001, *J. Astrophys. Astr.*, **22**, 21.

Bharadwaj, S., Sethi, S. K. 2001, *J. Astrophys. Astr.*, **22**, 293.

Bharadwaj, S., Pandey, S. K. 2003, *J. Astrophys. Astr*, **24**, 23.

Bharadwaj, S., Srikant, P. S. 2004, *J. Astrophys. Astr*, **25**, 67.

Bharadwaj, S., Sarkar, A. K., Ali, S. S. 2015, *J. Astrophys. Astr.*, **36**, 385.

Bowman, J. D. *et al.* 2013, *PASA*, **30**, 31.

Bull *et al.* 2015, *ApJ*, **803**, 21.

Chang, T.-C., Pen, U.-L., Peterson, J. B., McDonald, P. 2008, *Phys Rev. Lett.*, **100**, 091303.

Chang, T.-C., Pen, U.-L., Bandura, K., Peterson, J. B. 2010, *Nature*, **466**, 463.

Chatterjee, S., Bharadwaj, S., Marthi, V. R. 2017, *J. Astrophys. Astr.*, this issue.

DeBoer, D. *et al.* 2016, arXiv:1606:07473.

Delhaize, J., Meyer, M. J., Staveley-Smith, L., Boyle, B. J. 2013, *MNRAS*, **433**, 1398.

Dodelson, S. 2003, *Modern Cosmology*, Chapter 11.

Eisenstein, D. J., Hu, W. 1998, *ApJ*, **496**, 605.

Ewall-Wice, A., Hewitt, J., Mesinger, A., Dillon, J. S., Liu, A., Pober, J. 2016, *MNRAS*, **458**, 2710.

Ghelot, B. K. Bagla, J. S. 2017, *J. Astrophys. Astr.*, this issue.

Ghosh, A., Bharadwaj, S., Ali, S. S., Chenglur, J. N. 2011, *MNRAS*, **418**, 2584.

Guha Sarkar, T., Hazra, D. K. 2013, *JCAP*, **04**, 002.

Guha Sarkar, T., Mitra, S., Majumdar, S., Roy Choudhury, T. 2012, *MNRAS*, **421**, 3570.

Guha Sarkar, T., Datta, K. K. 2015, *JCAP*, **8**, 001.

Harker, G., Zaroubi, S., Bernardi, G., Brentjens, M. A. *et al.* 2010, *MNRAS*, **405**, 2492.

Kaiser, N. 1987, *MNRAS*, **227**, 1.

Lah, P. *et al.* 2007, *MNRAS*, **376**, 1357.

Loeb, A., Wyithe, J. S. B. 2008, *PRL*, **100**, 161301.

Mao, X.-C. 2012, *ApJ*, **744**, 29.

Martin, A. M., Papastergis, E., Giovanelli, R., Haynes, M. P., Springob, C. M., Stierwalt, S. 2010, *ApJ*, **723**, 1359.

Marthi, V. R., Chengalur, J. N. 2014, *MNRAS*, **437(1)**, 524.

Marthi, V. R., Chatterjee, S., Chengalur, J. N., Bharadwaj, S. 2017, *MNRAS* (submitted).

Marthi, V. R., 2017, *J. Astrophys. Astr.*, this issue.

Masui, K. W. *et al.* 2013, *ApJ*, **763**, L20.

McQuinn, M., Zahn, O., Zaldariagga, M., Hernquist, L., Furlanetto, S. R. 2006, *ApJ*, **653**, 815.

Meiring, J. D. *et al.* 2011, *ApJ*, **732**, 35.

Morales, M. F. 2005, *Ap.J*, **619**, 678.

Noterdaeme, P. *et al.* 2012, *A&A*, **547**, L1.

Neben, A. R., *et al.* 2016, arXiv:1602.03887.

Pal, A. K., Guha Sarkar, T. 2016, *MNRAS*, **459**, 3505.

Parsons, A. R. *et al.* 2010, *AJ*, **139**, 1468.

Parsons, A., Pober, J., McQuinn, M., Jacobs, D., Aguirre, J. 2012, *ApJ*, **753**, 81.

Pober, J. C., Parsons, A. R., DeBoer, D. R., McDonald, P., McQuinn, M., Aguirre, J. E., Ali, Z., Bradley, R. F., Chang, T.-C., Morales, M. F. 2013, *AJ*, **145**, 65.

Pober, J. C., Liu, A., Dillon, J. S., Aguirre, J. E., Bowman, J. D., Bradley, R. F., Carilli, C. F., DeBoer, D. R., Hewitt, J. N., Jacobs, D. C., McQuinn, M., Morales, M. F., Parsons, A. R., Tegmark, M., Werthimer, D. J. 2014, *ApJ*, **782**, 66.

Prasad, P., Subrahmanya, C. R. 2011a, arXiv:1102.0148, Presented at the Student Research Symposium of the 17th IEEE Conference on High Performance Computing, Dec 19–22, Goa, India.

Prasad, P., Subrahmanya, C. R. 2011b, *Exper. Astron.*, **31**, 1.

Prochaska, J. X., Wolfe, A. M. 2009, *ApJ*, **696**, 1543.

Rao, S. M., Turnshek, D. A., Nestor, D. B. 2006, *ApJ*, **636**, 610.

Rhee, J., Zwaan, M. A., Briggs, F. H., Chengalur, J. N., Lah, P., Oosterloo, T., van der Hulst, T. 2013, *MNRAS*, **435**, 2693.

Santos, M. G., Bull, P., Alonso, D., Camera, S., Ferreira, P. G., Bernardi, G., Marteens, R., Viel, M., Villaescusa-Navarro, F., Abdalla, F. B., Jarvis, M., Metcalf, R. B., Portsidou, A., Wolz, L. 2014, SKA Cosmology Chapter, *Advancing Astrophysics with the SKA (AASKA14), Conference, Giardini Naxos (Italy), June 9–13*.

Sarkar, D., Bharadwaj, S., Anathpindika, S. 2016, *MNRAS*, doi: 10.1093/mnras/stw1111.

Sarma, N. V. G., Joshi, M. N., Bagri, D. S., Ananthakrishnan, S. 1975, *J. Instn. Electron. Telecommun. Eng.*, **21**, 110.

Seo, H.-J., Dodelson, S., Marriner, J. *et al.* 2010, *ApJ*, **721**, 164.

Shaw, J. R., Sigurdson, K., Sitwell, M., Stebbins, A., Pen, Ue-Li 2015, *PRD*, **91**, 083514.

Shaw, J. R., Sigurdson, K., Pen, Ue-Li, Stebbins, A., Sitwell, M. 2014, *ApJ*, **781**, 57.

Subrahmanya, C. R., Prasad, P., Girish, B. S., Somasekahr, R., Manohara, P. K., Amit Mittal, S. G. 2017a, *J. Astrophys. Astr.*, this issue.

Subrahmanya, C. R., Manoharan, P. K., Chengalur, J. N. 2017b, *J. Astrophys. Astr.*, this issue.

Switzer, E. R. *et al.* 2013, *MNRAS*, **434**, L46.

Swarup, G., Sarma, N. V. G., Joshi, M. N., Kapahi, V. K., Bagri, D. S., Damle, S. H., Ananthakrishnan, S., Balasubramanian, V., Bhave, S. S., Sinha, R. P. 1971, *Nat. Phys. Sci.*, **230**, 185.

Swarup, G., Ananthakrishnan, S., Kapahi, V. K., Rao, A. P., Subrahmanya, C. R., Kulkarni, V. K. 1991, *Curr. Sci.*, **60**(**2**).

Tingay, S. *et al.* 2013, *PASA*, **30**, 7.

van Haarlem, M. P., Wise, M. W., Gunst, A. W. *et al.* 2013, *A&A*, **556**, A2.

Visbal, E., Loeb, A., Wyithe, S. 2009, *JCAP*, **10**, 30.

Villaescusa-Navarro, F., Bull, P., Viel, M. 2015, *ApJ*, **814**, 146.

Wyithe, J. S. B., Loeb, A. 2009, *MNRAS*, **397**, 1926.

Wyithe, J. S. B., Loeb, A., Geil, P. M. 2008, *MNRAS*, **383**, 1195.

Zwaan, M. A., Meyer, M. J., Staveley-Smith, L., Webster, R. L. 2005, *MNRAS*, **359**, L30.

Zafar, T., Peroux, C., Popping, A., Milliard, B., Deharveng, J.-M., Frank, S. 2013, *A&A*, **556**, A141.